

Effect of Imidazole Arrangements on Proton-Conductivity in Metal–Organic Frameworks

Feng-Ming Zhang,^{†,‡,§,¶} Long-Zhang Dong,^{†,‡,¶} Jun-Sheng Qin,^{§,¶} Wei Guan,[⊥] Jiang Liu,[†] Shun-Li Li,[†] Meng Lu,[†] Ya-Qian Lan,^{*,†,¶} Zhong-Min Su,^{⊥,¶} and Hong-Cai Zhou^{*,§,¶}

[†]Jiangsu Collaborative Innovation Centre of Biomedical Functional Materials, Jiangsu Key Laboratory of New Power Batteries, School of Chemistry and Materials Science, Nanjing Normal University, Nanjing 210023, P. R. China

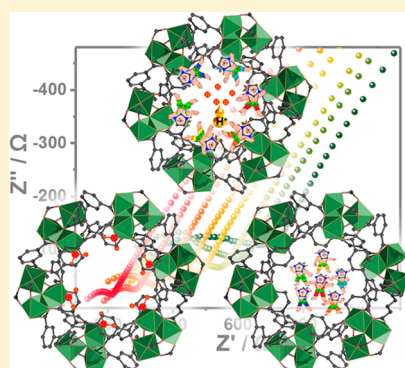
[‡]College of Chemical and Environmental Engineering, Harbin University of Science and Technology, Harbin 150040, P. R. China

[§]Department of Chemistry, Department of Materials Science and Engineering, Texas A&M Energy Institute, Texas A&M University, College Station, Texas 77843-3255, United States

[⊥]Department of Chemistry, Northeast Normal University, Changchun 130024, P. R. China

S Supporting Information

ABSTRACT: Imidazole molecules were frequently incorporated into porous materials to improve their proton conductivity. To investigate how different arrangements of imidazoles in metal–organic frameworks (MOFs) affect the overall proton conduction, we designed and prepared a MOF-based model system. It includes an Fe–MOF as the blank, an imidazole@Fe–MOF (Im@Fe–MOF) with physically adsorbed imidazole, and an imidazole–Fe–MOF (Im–Fe–MOF), which contains chemically coordinated imidazole molecules. The parent Fe–MOF, synthesized from the exchange of carboxylates in the preformed $[\text{Fe}_3(\mu_3\text{-O})](\text{carboxylate})_6$ clusters and multitopic carboxylate ligands, serves as a control. The Im@Fe–MOF was prepared by encapsulating free imidazole molecules into the pores of the Fe–MOF, whereas the Im–Fe–MOF was obtained in situ, in which imidazole ligands coordinate to the metal nodes of the framework. Proton-conductivity analyses revealed that the proton conductivity of Im–Fe–MOF was approximately two orders of magnitude greater than those of Fe–MOF and Im@Fe–MOF at room temperature. The high proton conductivity of $1.21 \times 10^{-2} \text{ S cm}^{-1}$ at 60 °C for Im–Fe–MOF ranks among the highest performing MOFs ever reported. The results of the density functional theory calculations suggest that coordinated imidazole molecules in Im–Fe–MOF provide a greater concentration of protons for proton transportation than do coordinated water molecules in Fe–MOF alone. Besides, Im–Fe–MOF exhibits steadier performance than Im@Fe–MOF does after being washed with water. Our investigation using the above ideal crystalline model system demonstrates that compared to disorderly arranged imidazole molecules in pores, the immobilized imidazole molecules by coordination bonds in the framework are more prone to form proton-conduction pathways and thus perform better and steadier in water-mediated proton conduction.



■ INTRODUCTION

As the most promising candidate among fuel cells for transportation applications, proton exchange membrane fuel-cells (PEMFCs) have attracted considerable interest of researchers.¹ Within PEMFCs, solid-state proton conductors are a crucial component that should be specifically designed to allow the exclusive diffusion of protons.² Commercial Nafion membranes for PEMFCs can attain proton conductivities of 10^{-1} – $10^{-2} \text{ S cm}^{-1}$ under 60–80 °C and 98% relative humidity (RH).³ However, the high manufacturing cost of Nafion and its narrow working conditions limit its wide-spread use.⁴ At the same time, the amorphous nature of Nafion polymers prevents any in-depth investigation of proton-conduction pathways and mechanisms, which make improving its proton conductivity difficult. In response, great effort has been devoted to exploring new inexpensive proton conductors with well-defined structure so as to endow fuel cells with better performance.⁵

Metal–organic frameworks, as a class of porous and crystalline materials composed of metal ions and organic linkers, have attracted vast attention of researchers in the field of proton conduction.⁶ The crystalline nature of MOFs allows the precise identification of their structural information to provide useful insights into proton-conduction pathways and mechanisms that are vital to designing new proton conductors. Moreover, the high tunability and designability of MOFs provide a platform for controlling and even improving proton conductivity. Yet, for MOF-based proton conductors, water and wide pH tolerances are crucial factors that should be taken into account preferentially since most reported MOFs easily collapse in those conditions.^{6b,7} To construct proton-conducting MOFs in which proton donors and acceptors are

Received: February 14, 2017

Published: April 7, 2017

arrayed to build proton pathways, two distinct strategies can be adopted as reported. The first approach involves the introduction of acidic groups into the framework backbones by reserving uncoordinated acid groups or converting the precursor groups into acidic groups with post-synthesis approach.^{6a,8} The second strategy involves the encapsulation of functional guest molecules (e.g., imidazole, triazole, histamine, ammonium cations, or involatile acids) into the pore spaces of MOFs to increase the concentration of protons in the material.^{6d,9} However, it is still ambiguous about how the distribution and arrangement of functional species or groups would affect the proton conduction in MOFs. Systematic analyses and comparisons of how arrangement of functional species or groups affect proton conduction are thus critical for better designing new proton-conducting materials.

In this context, we designed and prepared a MOF-based model system to investigate how functional species affect proton conductivities. We selected imidazole as a typical functional species, given its wide incorporation into various porous materials such as MOFs,^{9b,10} covalent organic frameworks (COFs),¹¹ and polymers to improve proton conductivity.¹² Our model system includes three compounds with the same host framework: Fe–MOF, Im@Fe–MOF, and Im–Fe–MOF. We built iron MOFs with $[\text{Fe}^{\text{III}}_2\text{Fe}^{\text{II}}(\mu_3\text{-O})]$ nodes as a model framework given iron MOFs' typically high stability, and our previous work that has demonstrated their possible preparation with $[\text{Fe}^{\text{III}}_2\text{Fe}^{\text{II}}(\mu_3\text{-O})(\text{CH}_3\text{COO})_6(\text{H}_2\text{O})_3]$ (hereafter $\text{Fe}_3\text{O}(\text{CH}_3\text{CO}_2)_6$) cluster as a starting material.¹³ Besides, three-coordinated water in the building block could be neutrally substituted by imidazole molecules to increase proton concentration of the framework. Proper ligand was also finely selected to ensure that the resulting pores or channels in the framework are large enough to accommodate imidazole, while the distance between the adjacent imidazole molecules would be appropriate for constructing hydrogen-bonding networks. The porous Fe–MOF was synthesized by the reaction between $\text{Fe}_3\text{O}(\text{CH}_3\text{CO}_2)_6$ clusters and multicarboxylic acid ligands. Im@Fe–MOF and Im–Fe–MOF were obtained via loading imidazole into the pores of the framework and anchoring imidazole to metal nodes by in situ reaction, respectively. These compounds are very stable in water and different pH solutions. Proton conductive analyses indicate that the coordinated imidazole molecules in Im–Fe–MOF facilitate the formation of proton-conductive pathway and greatly improve proton conductivity to approximately two orders of magnitude greater than that in Fe–MOF and Im@Fe–MOF at room temperature. The conductivity of $1.21 \times 10^{-2} \text{ S cm}^{-1}$ at 60 °C within Im–Fe–MOF is comparable to that of Nafion as well as several of the best performing MOF and COF materials under similar conditions.^{6a,d,9e,14} Additionally, Im–Fe–MOF could preserve its high proton conductivity after being washed with water three times, whereas the conductivity of Im@Fe–MOF rapidly decreased to the comparable value in Fe–MOF after being washed only once. The results with the MOF-based model system demonstrated that coordinated imidazole molecules in the framework better benefit proton conduction than those of disordered distribution in pores.

RESULTS AND DISCUSSION

Fe–MOF was synthesized by the reaction of $\text{Fe}_3\text{O}(\text{CH}_3\text{CO}_2)_6$ clusters and [1,1':3',1''-terphenyl]-4,4'',5'-tricarboxylic acid (H_3L) ligands under solvothermal condition with acetic acid

as the competing reagent. X-ray crystallographic analysis reveals that Fe–MOF crystallizes in the trigonal system with $R\bar{3}c$ space group and the asymmetric unit contains one L^{3-} ligand, one and a half Fe ions, a half $\mu_3\text{-O}^{2-}$, and one and a half coordinated H_2O molecules (Figure S1). As shown in Figure 1a

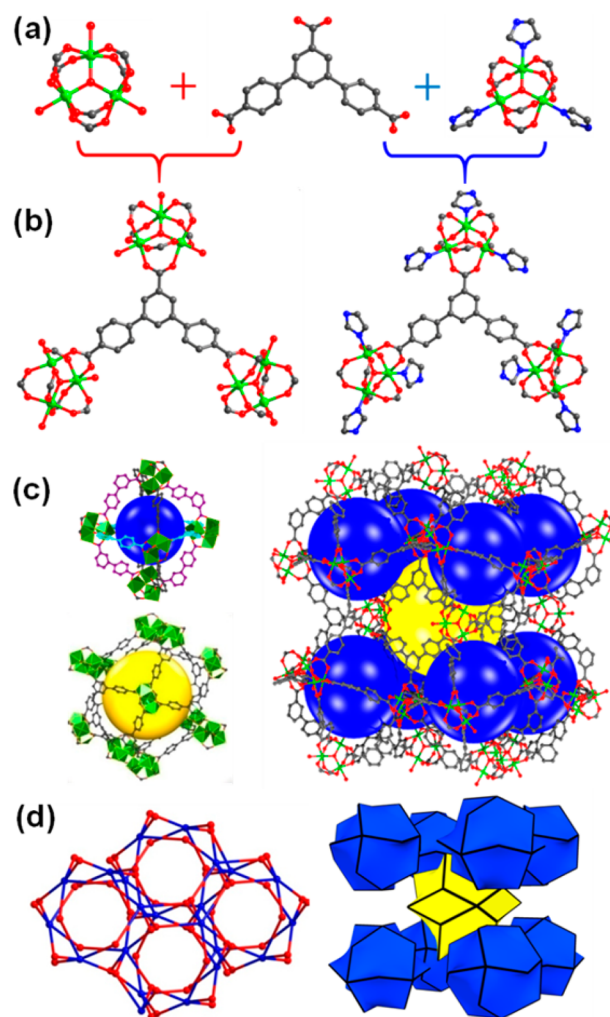


Figure 1. (a) Ligand used in this work, and the trinuclear metal clusters in Fe–MOF and Im–Fe–MOF, respectively. (b) Connection mode of ligands with metal clusters in Fe–MOF and Im–Fe–MOF. (c) Two types of hollow cages in Fe–MOF. (d) Topological analysis of Fe–MOF.

and b, each L^{3-} ligand in Fe–MOF connects three metal clusters. Six CH_3COO^- groups in the precursor cluster were fully substituted by COO^- groups from six different ligands, while three-coordinated H_2O molecules were finally reserved (Figure S2). The prime network of Fe–MOF consists of two different types of hollow cages: the smaller cage was formed by six metal clusters connected by ligands with an accessible diameter of about 13.2 Å, while the bigger cage was formed by 12 metal clusters and ligands with an accessible diameter of about 22.1 Å (Figure 1c). Each big cage was surrounded by eight small cages, and such connectivity pattern was repeated infinitely to assemble the 3D framework. The framework exhibits circular 1D channel along the *c* axis direction with the diameter of about 10.0 Å (Figure S3). The structure of Im–Fe–MOF is similar to that of Fe–MOF except that coordinated water molecules in the metal nodes were fully

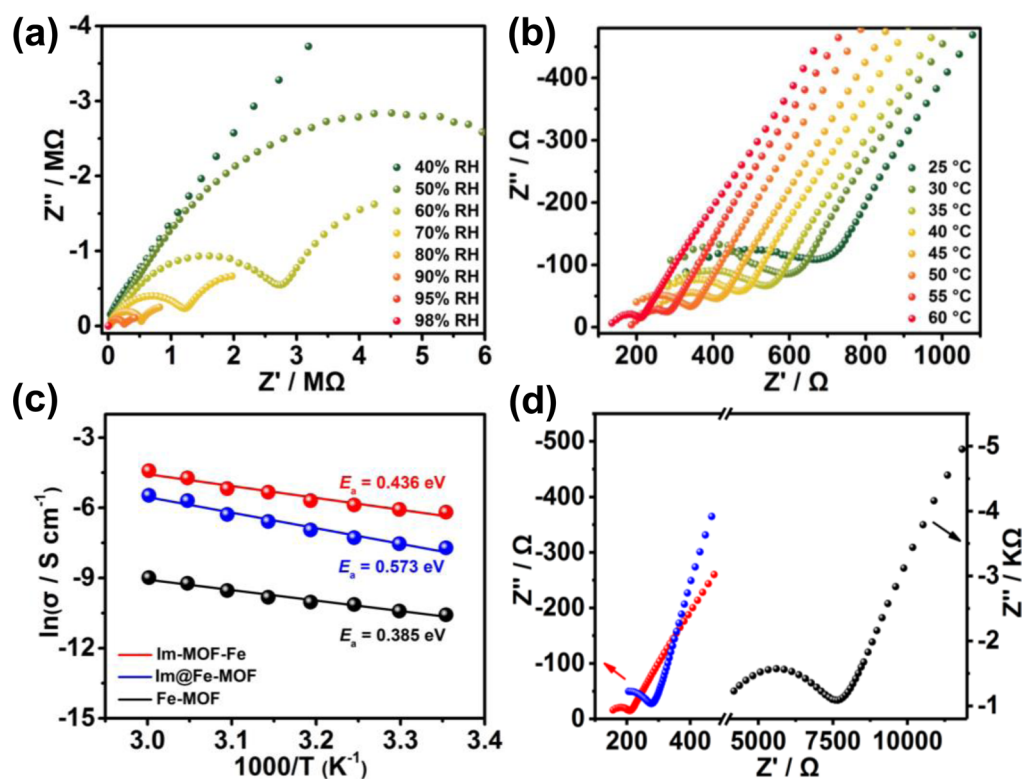


Figure 2. (a) Impedance spectrum of Im-Fe-MOF at 25 °C with different RHs. (b) Impedance spectrum of Im-Fe-MOF under 98% RH with different temperatures. (c) Arrhenius plots of proton conductivity for Fe-MOF, Im@Fe-MOF, and Im-Fe-MOF under 98% RH conditions. (d) Comparison of impedance spectra for Fe-MOF (black), Im@Fe-MOF (blue), and Im-Fe-MOF (red) under 60 °C with 98% RH.

substituted by imidazole molecules (Figures 1a,b and S1). Interestingly, the coordinated imidazole molecules in Im-Fe-MOF stretch toward the interior of cage, which further narrow the 1D channel to 5.6 Å viewed along the *c* axis (Figure S3). Notably, imidazole molecules in the Im-Fe-MOF just neutrally coordinate to replace the sites of water, and hydrogen atom bonded to nitride atom of imidazole is entirely preserved. Calculation by PLATON software reveals that the free volumes are up to 72.3% and 66.7% in Fe-MOF and Im-Fe-MOF, respectively.¹⁵ Topological analysis using TOPOS software identified that the framework has a new 3,6-c 2-nodal net topology with the Schläfli symbol $\{4.6^2\}_2\{4^2.6^7.8^6\}$ (Figure 1d),¹⁶ which is unknown in Reticular Chemistry Structure Resource (RCSR) database.

The phase purities of the as-synthesized Fe-MOF and Im-Fe-MOF were confirmed by matching powder X-ray diffraction (PXRD) patterns with their simulated patterns from single crystal X-ray diffraction (Figures S5 and S6). To investigate pH stability of these two compounds, the samples were immersed in different pH aqueous solutions for 24 h, and the identical PXRD patterns before and after immersed demonstrated that these two compounds could preserve their structural integrity covering the pH range from 1–12. The excellent water stability of Im-Fe-MOF was further confirmed by overlapping the PXRD profile of the sample immersed in water for three months with the simulated PXRD pattern (Figure S7). Variable temperature PXRD patterns of Fe-MOF and Im-Fe-MOF demonstrated that these two compounds could preserve their structural integrity up to 350 °C (Figures S8 and S9). For Im@Fe-MOF, obtained by immersing Fe-MOF into a concentrated imidazole solution in methanol solution, the PXRD pattern was identical with its that of parent

Fe-MOF, meaning the framework has no change before and after imidazole loading (Figure S10). The results of X-ray photoelectron spectroscopy (XPS) for these three compounds demonstrated that imidazole molecules in Im@Fe-MOF did not coordinate to metal nodes after imidazole loading (Figures S11–S13).¹⁷

Thermogravimetric analyses under O₂ atmosphere also revealed that these three materials have thermal stability up to ~350 °C (Figure S14). From the results of TGA and elemental analysis, the weight percentage of imidazole loading in Im@Fe-MOF was estimated to be ~20 wt %, which corresponded to ~63 imidazole molecules per crystal cell of the framework, and slightly higher than 54 imidazole molecules in the unit cell of Im-Fe-MOF observed from structural data. The porosity of three compounds was investigated by N₂ absorption and desorption experiments at 77 K. All of the absorption isotherms exhibit type I isotherm according to the IUPAC classification (Figure S15). The saturated uptakes for Fe-MOF, Im@Fe-MOF, and Im-Fe-MOF are 964.80, 638.77, and 711.19 cm³ g⁻¹, while the Brunauer–Emmett–Teller (BET) surface areas are 2109.62, 1894.41, and 1627.71 m² g⁻¹, respectively. Evaluations of density functional theory (DFT) simulation from the N₂ absorption curves indicate that the pore sizes are 0.92, 0.83, and 0.88 nm for Fe-MOF, Im@Fe-MOF, and Im-Fe-MOF, respectively. All the results of N₂ absorption experiments are in agreement with structural information.

Proton conductivity of Fe-MOF, Im@Fe-MOF, and Im-Fe-MOF was determined by alternating current (AC) impedance spectroscopy. The conductivity of each sample was measured at 25 °C with varying humidities to elucidate the correlation between conductivity and relative humidity (Figures

2a, S16, and S17). At 40% RH, the conductivity of Fe–MOF was found to be a negligible value of $1.28 \times 10^{-9} \text{ S cm}^{-1}$. With RH increasing, proton conductivity of Fe–MOF further increased to $2.56 \times 10^{-5} \text{ S cm}^{-1}$ at 98% RH. At the same condition of 98% RH, the value of proton conductivity for Im@Fe–MOF is $8.41 \times 10^{-5} \text{ S cm}^{-1}$, while the conductivity of Im–Fe–MOF is high up to $2.06 \times 10^{-3} \text{ S cm}^{-1}$, which is about two orders of magnitude greater than that of the formers. The variation of proton conductivity with the increase of RH indicates that the process of proton conduction in these compounds is dominated by water-mediated proton conduction that is typically improved by orders of magnitude upon increasing RH, even in a narrow range of high RHs.^{14d,18}

To further understand the role of humidity in proton conduction in these compounds, water vapor absorption and desorption isotherms for these compounds were measured at 25 °C (Figure S18). The absorption isotherm of Fe–MOF reaches a maximum water vapor uptake of $616.21 \text{ cm}^3 \text{ g}^{-1}$, which is much higher than that in Im@Fe–MOF ($390.14 \text{ cm}^3 \text{ g}^{-1}$) and Im–Fe–MOF ($342.56 \text{ cm}^3 \text{ g}^{-1}$). The lower water vapor absorptions in Im@Fe–MOF and Im–Fe–MOF result from the occupation of free imidazole molecules in the pores of the framework and the coordinated imidazole molecules in the metal nodes, respectively. It can be speculated that the large water vapor absorption in Fe–MOF is more favorable for the formation of hydrogen-bonded water networks in the structure. All of the water vapor absorption isotherms for these three compounds exhibit obvious two-step pore-filling uptake of water vapor, with the first pore-filling step starting around 40% low humidity and the second beginning around 80% high RH. This two-step process of water absorption observed in these compounds may arise from the filling of the 13.2 Å pores followed by that of the 22.1 Å pores in their frameworks.¹⁹ All samples exhibited hysteresis loop between the adsorption and desorption branches. The second water uptake step at high RH in Fe–MOF and Im–Fe–MOF should be responsible for their rapid increases of proton conductivity up 90% RH.^{6c,14c,20} The structural integrities were identified by the PXRD patterns before and after water vapor absorption measurements (Figure S19).

The temperature dependence of the proton conductivity for these samples was measured in the temperature range of 25–60 °C (Figures 2b and S20–S23). Upon the increasing temperature, the optimized proton conductivities for Fe–MOF, Im@Fe–MOF, and Im–Fe–MOF were determined to be 1.25×10^{-4} , 4.23×10^{-3} , and $1.21 \times 10^{-2} \text{ S cm}^{-1}$, respectively, under 60 °C and 98% RH. The remarkable proton conductivity ($1.21 \times 10^{-2} \text{ S cm}^{-1}$) of Im–Fe–MOF is comparable to that of Nafion as well as several of the highest performing MOFs materials under similar conditions (see Table S1). Moreover, the structural integrities of these compounds were confirmed by the PXRD patterns before and after impedance analyses (Figure S24). The activation energies of these compounds were determined from least-squares fits of the slopes to gain insights into the proton-conduction mechanism (Figures 2c and S25–S26). Under 98% RH, the yield activation energy values (E_a) for Fe–MOF, Im@Fe–MOF, and Im–Fe–MOF are 0.385, 0.573, and 0.436 eV, respectively. According to Grotthuss mechanism and Vehicle mechanism used to explain proton conduction,²¹ typical reported activation energies are 0.1–0.4 eV for the Grotthuss mechanism and 0.5–0.9 eV for the Vehicle mechanism,²² which suggest that different proton conductive mechanisms may exist in these three compounds.

The results of structural analysis, activation energy, and water vapor absorption of these three compounds were utilized to further get an insight into the proton pathways and mechanisms in them. For Fe–MOF, it can be concluded that the absorbed water molecules themselves or together with coordinated water molecules could easily construct rich hydrogen-bonded networks in the channels of the framework for proton hopping, resulting a lower E_a and Grotthuss mechanism in proton conduction. However, the pore space in Im@Fe–MOF was mainly occupied by disordered imidazole molecules and accompanied by much lower water vapor absorption than Fe–MOF, which may block the formation of successive hydrogen bonding networks serving as proton conduction pathways. Thus, the proton conduction in Im@Fe–MOF is probably dominated by dynamic motion or rotation of guests in the channels, resulting in a high activation energy and Vehicular mechanism. The higher proton conductivity of Im@Fe–MOF compared to Fe–MOF should be attributed to imidazole molecules in the pores of the framework.

In comparison with Fe–MOF, Im–Fe–MOF also has narrower channels and lower water absorption capability for the occupation of regularly arranged imidazole molecules by coordination, different from the case in Im@Fe–MOF. To further gain an insight into the mechanism of proton conduction in Im–Fe–MOF, DFT calculations were applied by simplifying model of Fe–MOF and Im–Fe–MOF extracted from their crystal structures (Figure 3a and Computational Details in the Supporting Information). DFT calculations indicate that imidazole molecule could effectively replace the coordinated water in the metal nodes of Fe–MOF to generate Im–Fe–MOF. The replacement reaction was evaluated to be exothermic by $-23.0 \text{ kcal mol}^{-1}$ in aqueous solution. Furthermore, compared to water, the coordinated imidazole could be easier to contribute proton for the weak N–H bond. The binding energies of H(–OH) and H(–N₂C₃H₃) with the rest of Fe–MOF and Im–Fe–MOF are -112.1 and $-96.8 \text{ kcal mol}^{-1}$, respectively. In a word, the calculated results suggest that the coordinated imidazole not only enhances the stability of trinuclear Fe cluster, but also improves the concentration of proton. In the structure of Im–Fe–MOF, the distances between neighboring imidazole molecules along the channel of *c* axis direction are about 7.735 and 14.496 Å. This means that successive hydrogen-bonding networks could not be built solely by coordinated imidazole molecules in Im–Fe–MOF. The proton-hopping pathways could be formed by combining imidazole and absorbed water molecules, resulting in Grotthuss mechanism (Figure 3b). Meantime, the absorbed water molecules also have the possibility to accept protons from imidazole and transport protons through self-diffusion, resulting in partly Vehicular mechanism for the conduction. Thus, it is expected that a mixed mechanism, Grotthuss mechanism and partially Vehicular mechanism, likely occurs in Im–Fe–MOF.²³

Since the electrochemical reaction in hydrogen and methanol fuel cells would generate water at the cathode,²⁴ stable performance of the proton exchange materials under moisture and water atmosphere is highly expected. To evaluate the proton-conductive stability of these compounds suffering from water immersion, we washed each sample with water for three times and then measured the variation of impedance each time. The proton conductivity for Fe–MOF, Im@Fe–MOF, and Im–Fe–MOF corresponded to washing times were shown in

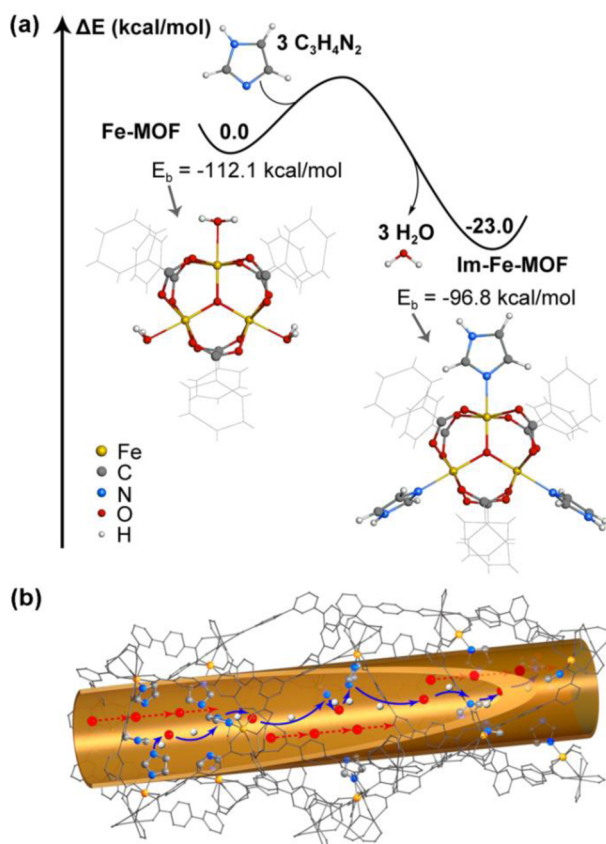


Figure 3. (a) Reaction energy of ligand exchange (ΔE , in kcal mol⁻¹) calculated at the CPCM(water)/UB3LYP/[6-311++G(d,p)/SDD-(Fe)]/UB3LYP/[6-31G(d)/LANL2DZ(Fe)] level. (b) Schematic view of possible proton-conductive pathways in Im-Fe-MOF. Water molecules are shown in red. Blue arrows show the protons hop along hydrogen-bonding networks formed by coordinated imidazole and absorbed water. Red arrows represent transport of protons through self-diffusion of protonated water.

Figure 4. As we can see, the proton conductivity of Fe-MOF and Im-Fe-MOF has no apparent change after three times of wash. However, the conductivity of Im@Fe-MOF decreased largely to the comparable value with that of Fe-MOF even after washing with water for only once. These results demonstrate that the immobilized imidazole molecules in the framework not only facilitate the water-mediated proton conduction, but also sustain the stable performance of proton conduction in Im-Fe-MOF for avoiding the permeation of proton carriers under water atmosphere.

CONCLUSIONS

In conclusion, we successfully established a Fe-MOF-based model system to investigate the influence of imidazole on proton conduction. The ultra-stable and porous Fe-MOF with trinuclear metal nodes provides an ideal platform for the construction of the model system. Two other materials in the model system, Im@Fe-MOF and Im-Fe-MOF, were formed by loading imidazole into the pores of the framework and by coordinating imidazole with the metal nodes, respectively. The proton conductivity of Im-Fe-MOF is approximately two orders of magnitude greater than those of Im@Fe-MOF and Fe-MOF under the same conditions. Different proton-conducting mechanisms occurred in them and the corresponding proton-conductive pathways were discussed according to

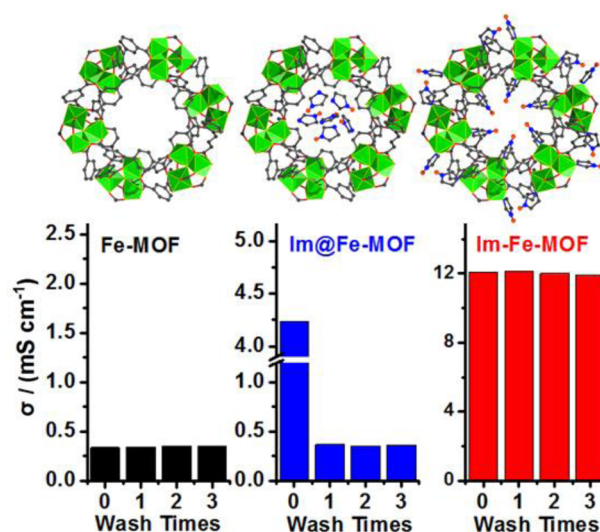


Figure 4. Variation of proton conductivities with wash times of samples for Fe-MOF, Im@Fe-MOF, and Im-Fe-MOF, respectively. Corresponding impedance analyses were measured under 60 °C and 98% RH.

DFT calculations and experimental results. Furthermore, Im-Fe-MOF has very stable performance under water atmosphere contributed from the immobilized imidazole by coordination bonds, while the conductivity of Im@Fe-MOF would decrease to a comparable value with that in Fe-MOF after being washed once with water due to the leaching of imidazole. These detailed investigations by utilizing the ideal crystalline model system demonstrate that the immobilized and regularly arranged imidazole in the framework by coordination bonds could be more helpful for the formation of proton-conductive pathways under humidity condition comparing to the imidazole molecules with disordered distribution in pore spaces. This investigation results are meaningful for understanding the proton conduction affected by imidazole and instructive for further design of new proton-conducting materials.

ASSOCIATED CONTENT

Supporting Information

The Supporting Information is available free of charge on the ACS Publications website at DOI: 10.1021/jacs.7b01559.

Detailed information regarding the experimental methods, syntheses, powder XRD patterns, gas sorption, impedance analysis (PDF)
CIF file for Fe-MOF (CIF)
CIF file for Im-Fe-MOF (CIF)

AUTHOR INFORMATION

Corresponding Authors

*yqlan@nynu.edu.cn
*zhou@chem.tamu.edu

ORCID

Long-Zhang Dong: 0000-0002-9276-5101
Ya-Qian Lan: 0000-0002-2140-7980
Zhong-Min Su: 0000-0002-3342-1966
Hong-Cai Zhou: 0000-0002-9029-3788

Author Contributions

[†]F.-M.Z., L.-Z.D., and J.-S.Q. contributed equally to this work.

Notes

The authors declare no competing financial interest.

■ ACKNOWLEDGMENTS

This work was financially supported by the National Natural Science Foundation of China (Nos. 21622104, 21371099, 21471080, and 21501036), the NSF of Jiangsu Province of China (No. BK20141445), the Priority Academic Program Development of Jiangsu Higher Education Institutions, the Foundation of Jiangsu Collaborative Innovation Center of Biomedical Functional Materials, and Jiangsu Planned Projects for Postdoctoral Research Funds (1601072B). We acknowledge Dr. Gang Xu (Fujian Institute of Research on the Structure of Matter, Chinese Academy of Sciences) for fruitful discussions about proton conduction in this paper.

■ REFERENCES

- (1) (a) Jacobson, M. Z.; Colella, W. G.; Golden, D. M. *Science* **2005**, *308*, 1901. (b) Wang, Y.; Chen, K. S.; Mishler, J.; Cho, S. C.; Adroher, X. C. *Appl. Energy* **2011**, *88*, 981. (c) Simonsson, D. *Chem. Soc. Rev.* **1997**, *26*, 181. (d) Ellingsen, L. A.-W.; Hung, C. R.; Majeau-Bettez, G.; Singh, B.; Chen, Z.; Whittingham, M. S.; Stromman, A. H. *Nat. Nanotechnol.* **2016**, *11*, 1039. (e) Steele, B. C. H.; Heinzel, A. *Nature* **2001**, *414*, 345.
- (2) (a) Shimizu, G. K. H.; Taylor, J. M.; Kim, S. R. *Science* **2013**, *341*, 354. (b) Kreuer, K.-D.; Paddison, S. J.; Spohr, E.; Schuster, M. *Chem. Rev.* **2004**, *104*, 4637. (c) Liu, M.; Chen, L.; Lewis, S.; Chong, S. Y.; Little, M. A.; Hasell, T.; Aldous, I. M.; Brown, C. M.; Smith, M. W.; Morrison, C. A.; Hardwick, L. J.; Cooper, A. I. *Nat. Commun.* **2016**, *7*, 12750. (d) Nasef, M. M. *Chem. Rev.* **2014**, *114*, 12278. (e) Scofield, M. E.; Liu, H.; Wong, S. S. *Chem. Soc. Rev.* **2015**, *44*, 5836.
- (3) (a) Laberty-Robert, C.; Valle, K.; Pereira, F.; Sanchez, C. *Chem. Soc. Rev.* **2011**, *40*, 961. (b) Mauritz, K. A.; Moore, R. B. *Chem. Rev.* **2004**, *104*, 4535. (c) Li, Q.; He, R.; Jensen, J. O.; Bjerrum, N. J. *Chem. Mater.* **2003**, *15*, 4896.
- (4) (a) Yoon, M.; Suh, K.; Natarajan, P. S.; Kim, P. K. *Angew. Chem.* **2013**, *125*, 2752. (b) Dong, B.; Gwee, L.; Salas-de la Cruz, D.; Winey, K. I.; Elabd, Y. A. *Nano Lett.* **2010**, *10*, 3785.
- (5) (a) Sadakiyo, M.; Yamada, T.; Kitagawa, H. *ChemPlusChem* **2016**, *81*, 691. (b) Pili, S.; Argent, S. P.; Morris, C. G.; Rought, P.; Garciasakai, V.; Silverwood, I. P.; Easun, T. L.; Ming, L.; Warren, M. R.; Murray, C. A.; et al. *J. Am. Chem. Soc.* **2016**, *138*, 6352. (c) Luo, H.-B.; Ren, L.-T.; Ning, W.-H.; Liu, S.-X.; Liu, J.-L.; Ren, X.-M. *Adv. Mater.* **2016**, *28*, 1663. (d) Borges, D. D.; Devautour-Vinot, S.; Jobic, H.; Ollivier, J.; Nouar, F.; Semino, R.; Devic, T.; Serre, C.; Paesani, F.; Maurin, G. *Angew. Chem.* **2016**, *128*, 3987.
- (6) (a) Phang, W. J.; Jo, H.; Lee, W. R.; Song, J. H.; Yoo, K.; Kim, B. S.; Hong, C. S. *Angew. Chem., Int. Ed.* **2015**, *54*, 5142. (b) Wang, C.; Liu, X.; Keser Demir, N.; Chen, J. P.; Li, K. *Chem. Soc. Rev.* **2016**, *45*, 5107. (c) Sadakiyo, M.; Yamada, T.; Honda, K.; Matsui, H.; Kitagawa, H. *J. Am. Chem. Soc.* **2014**, *136*, 7701. (d) Nagarkar, S. S.; Unni, S. M.; Sharma, A.; Kurungot, S.; Ghosh, S. K. *Angew. Chem., Int. Ed.* **2014**, *53*, 2638. (e) Nguyen, N. T. T.; Furukawa, H.; Gándara, F.; Trickett, C. A.; Jeong, H. M.; Cordova, K. E.; Yaghi, O. M. *J. Am. Chem. Soc.* **2015**, *137*, 15394. (f) Hurd, J. A.; Vaidhyanathan, R.; Thangadurai, V.; Ratcliffe, C. L.; Moudrakovski, I. L.; Shimizu, G. K. H. *Nat. Chem.* **2009**, *1*, 705.
- (7) (a) Li, P.; Vermeulen, N. A.; Gong, X.; Malliakas, C. D.; Stoddart, J. F.; Hupp, J. T.; Farha, O. K. *Angew. Chem.* **2016**, *128*, 10514. (b) Guo, P.; Dutta, D.; Wong-Foy, A. G.; Gidley, D. W.; Matzger, A. J. *J. Am. Chem. Soc.* **2015**, *137*, 2651. (c) Burtch, N. C.; Walton, K. S. *Acc. Chem. Res.* **2015**, *48*, 2850.
- (8) (a) Taylor, J. M.; Dawson, K. W.; Shimizu, G. K. H. *J. Am. Chem. Soc.* **2013**, *135*, 1193. (b) Shigematsu, A.; Yamada, T.; Kitagawa, H. *J. Am. Chem. Soc.* **2011**, *133*, 2034. (c) Bazagarcia, M.; Colodrero, R. M. P.; Papadaki, M.; Garczarek, P.; Zóñ, J.; Oliverapastor, P.; Losilla, E. R.; Leónreina, L.; Aranda, M. A. G.; Choquesilolazarte, D.; et al. *J. Am. Chem. Soc.* **2014**, *136*, 5731. (d) Yang, F.; Huang, H.; Wang, X.; Li, F.; Gong, Y.; Zhong, C.; Li, J. R. *Cryst. Growth Des.* **2015**, *15*, 5827. (e) Ramaswamy, P.; Matsuda, R.; Kosaka, W.; Akiyama, G.; Jeon, H. J.; Kitagawa, S. *Chem. Commun.* **2014**, *50*, 1144. (f) Liang, X.; Zhang, F.; Feng, W.; Zou, X.; Zhao, C.; Na, H.; Liu, C.; Sun, F.; Zhu, G. *Chem. Sci.* **2013**, *4*, 983.
- (9) (a) Ponomareva, V. G.; Kovalenko, K. A.; Chupakhin, A. P.; Dybtsev, D. N.; Shutova, E. S.; Fedin, V. P. *J. Am. Chem. Soc.* **2012**, *134*, 15640. (b) Liu, S.; Yue, Z.; Liu, Y. *Dalton Trans.* **2015**, *44*, 12976. (c) Yamada, T.; Otsubo, K.; Makiura, R.; Kitagawa, H. *Chem. Soc. Rev.* **2013**, *42*, 6655. (d) Liu, Y.; Yang, X.; Miao, J.; Tang, Q.; Liu, S.; Shi, Z.; Liu, S. *Chem. Commun.* **2014**, *50*, 10023. (e) Chandra, S.; Kundu, T.; Kandambeth, S.; BabaRao, R.; Marathe, Y.; Kunjir, S. M.; Banerjee, R. *J. Am. Chem. Soc.* **2014**, *136*, 6570. (f) Liu, S.-J.; Cao, C.; Yang, F.; Yu, M.-H.; Yao, S.-L.; Zheng, T.-F.; He, W.-W.; Zhao, H.-X.; Hu, T.-L.; Bu, X.-H. *Cryst. Growth Des.* **2016**, *16*, 6776.
- (10) (a) Eisbein, E.; Joswig, J.-O.; Seifert, G. *Microporous Mesoporous Mater.* **2015**, *216*, 36. (b) Uneyama, D.; Horike, S.; Inukai, M.; Hijikata, Y.; Kitagawa, P. S. *Angew. Chem., Int. Ed.* **2011**, *50*, 11706. (c) Eisbein, E.; Joswig, J. O.; Seifert, G. *J. Phys. Chem. C* **2014**, *118*, 13035. (d) Bureekaew, S.; Horike, S.; Higuchi, M.; Mizuno, M.; Kawamura, T.; Tanaka, D.; Yanai, N.; Kitagawa, S. *Nat. Mater.* **2009**, *8*, 831.
- (11) Xu, H.; Tao, S.; Jiang, D. *Nat. Mater.* **2016**, *15*, 722.
- (12) Ye, Y.; Zhang, L.; Peng, Q.; Wang, G. E.; Shen, Y.; Li, Z.; Wang, L.; Ma, X.; Chen, Q. H.; Zhang, Z.; et al. *J. Am. Chem. Soc.* **2015**, *137*, 913.
- (13) (a) Feng, D.; Wang, K.; Wei, Z.; Chen, Y. P.; Simon, C. M.; Arvapally, R. K.; Martin, R. L.; Bosch, M.; Liu, T. F.; Fordham, S.; et al. *Nat. Commun.* **2014**, *5*, 5723. (b) Sudik, A. C.; Millward, A. R.; Ockwig, N. W.; Côté, A. P.; Kim, J.; Yaghi, O. M. *J. Am. Chem. Soc.* **2005**, *127*, 7110. (c) Wang, K.; Feng, D.; Liu, T. F.; Su, J.; Yuan, S.; Chen, Y. P.; Bosch, M.; Zou, X.; Zhou, H. C. *J. Am. Chem. Soc.* **2014**, *136*, 13983. (d) Serre, C.; Millange, F.; Surlle, S.; Férey, G. *Angew. Chem., Int. Ed.* **2004**, *43*, 6285. (e) Chevreau, H.; Devic, T.; Salles, F.; Maurin, G.; Stock, N.; Serre, C. *Angew. Chem., Int. Ed.* **2013**, *52*, S056. (f) Schoedel, A.; Zaworotko, M. J. *Chem. Sci.* **2014**, *5*, 1269. (g) Sudik, A. C.; Côté, A. P.; Wong-Foy, A. G.; O'Keeffe, M.; Yaghi, O. M. *Angew. Chem., Int. Ed.* **2006**, *45*, S2528.
- (14) (a) Phang, W. J.; Lee, W. R.; Yoo, K.; Ryu, D. W.; Kim, B. S.; Hong, C. S. *Angew. Chem., Int. Ed.* **2014**, *53*, 8383. (b) Kim, S. R.; Dawson, K. W.; Gelfand, B. S.; Taylor, J. M.; Shimizu, G. K. H. *J. Am. Chem. Soc.* **2013**, *135*, 963. (c) Ōkawa, H.; Sadakiyo, M.; Yamada, T.; Maesato, M.; Ohba, M.; Kitagawa, H. *J. Am. Chem. Soc.* **2013**, *135*, 2256. (d) Ramaswamy, P.; Wong, N. E.; Gelfand, B. S.; Shimizu, G. K. H. *J. Am. Chem. Soc.* **2015**, *137*, 7640. (e) Sen, S.; Nair, N. N.; Yamada, T.; Kitagawa, H.; Bharadwaj, P. K. *J. Am. Chem. Soc.* **2012**, *134*, 19432. (f) Peng, Y.; Xu, G.; Hu, Z.; Cheng, Y.; Chi, C.; Yuan, D.; Cheng, H.; Zhao, D. *ACS Appl. Mater. Interfaces* **2016**, *8*, 18505. (g) Chandra, S.; Kundu, T.; Dey, K.; Addicoat, M.; Heine, T.; Banerjee, R. *Chem. Mater.* **2016**, *28*, 1489. (h) Ma, H.; Liu, B.; Li, B.; Zhang, L.; Li, Y.-G.; Tan, H.-Q.; Zang, H.-Y.; Zhu, G. *J. Am. Chem. Soc.* **2016**, *138*, 5897.
- (15) Spek, A. L. *J. Appl. Crystallogr.* **2003**, *36*, 7.
- (16) Alexandrov, E. V.; Blatov, V. A.; Kochetkov, A. V.; Proserpio, D. M. *CrystEngComm* **2011**, *13*, 3947.
- (17) (a) Hendrickson, D. N.; Hollander, J. M.; Jolly, W. L. *Inorg. Chem.* **1969**, *8*, 2642. (b) Böhlend, H.; Hanay, W.; Meisel, A.; Scheibe, R. Z. *Chem.* **1981**, *21*, 372.
- (18) (a) Zhao, X.; Mao, C.; Bu, X.; Feng, P. *Chem. Mater.* **2014**, *26*, 2492. (b) Sadakiyo, M.; Ōkawa, H.; Shigematsu, A.; Ohba, M.; Yamada, T.; Kitagawa, H. *J. Am. Chem. Soc.* **2012**, *134*, 5472. (c) Dong, X. Y.; Wang, R.; Li, J. B.; Zang, S. Q.; Hou, H. W.; Mak, T. C. *Chem. Commun.* **2013**, *49*, 10590.
- (19) (a) Canivet, J.; Fateeva, A.; Guo, Y.; Coasne, B.; Farrusseng, D. *Chem. Soc. Rev.* **2014**, *43*, 5594. (b) Akiyama, G.; Matsuda, R.; Sato, H.; Hori, A.; Takata, M.; Kitagawa, S. *Microporous Mesoporous Mater.* **2012**, *157*, 89.
- (20) Tominaka, S.; Coudert, F. X.; Dao, T. D.; Nagao, T.; Cheetham, A. K. *J. Am. Chem. Soc.* **2015**, *137*, 6428.

- (21) (a) Kreuer, K. D.; Rabenau, A.; Weppner, W. *Angew. Chem., Int. Ed. Engl.* **1982**, *21*, 208. (b) Kreuer, K.-D. *Chem. Mater.* **1996**, *8*, 610.
- (22) Ramaswamy, P.; Wong, N. E.; Shimizu, G. K. *Chem. Soc. Rev.* **2014**, *43*, 5913.
- (23) Sadakiyo, M.; Yamada, T.; Kitagawa, H. *J. Am. Chem. Soc.* **2014**, *136*, 13166.
- (24) (a) Kreuer, K. D. *J. Membr. Sci.* **2001**, *185*, 29. (b) Haile, S. M. *Acta Mater.* **2003**, *51*, 5981.